Formation mechanism of self-assembled unilamellar vesicles[1]

Mu-Ping Nieh, Norbert Kučerka, and John Katsaras

Abstract: Uniform size self-assembled unilamellar vesicles (ULVs) can be produced from mixtures of weakly charged short- and long-chain phospholipids. These lipid mixtures self-assemble into bilayered micelles (so-called bicelles), and a bicelle to ULV transition has been previously reported. Here, we discuss the effect of various parameters (i.e., lipid concentration, charge density, membrane rigidity, lipid composition, and lipid hydrocarbon chain length) on ULV radius as determined by small angle neutron scattering (SANS). SANS data were best fit using a core-shell disk and a spherical-shell model to obtain the size of bicelles and ULVs, respectively. From the present experiments we conclude that a previously proposed mechanism of ULV formation, where bicelles coalesce into large precursor and self-fold into ULVs, is able to explain the present SANS data.

PACS No: 87.14.Cc

Résumé : Il est possible de produire des vésicules à une couche auto-assemblées et de grosseur uniforme (ULVs), à partir de mélanges de chaînes de phospholipides courtes et longues faiblement chargées. Ces mélanges de lipides s'auto-assemblent en micelles bicouches (parfois appelées bicelles) et une transition de bicelle à ULV a déjà été décrite. Nous discutons ici l'effet de différents paramètres (la concentration lipidique, la densité de charge, la rigidité de membrane, la composition lipidique et la longueur des chaînes lipidiques) sur le rayon des ULV qui est déterminé par diffusion de neutrons aux petits angles (SANS). Nous ajustons la courbe des données SANS à l'aide d'un modèle en couches sphériques pour obtenir la grosseur des bicelles et des ULV respectivement. À partir des présentes expériences, nous concluons qu'un mécanisme préalablement rapporté sur la formation des ULV, où les bicelles coalescent en un gros précurseur et s'auto-replient en ULV, est capable d'expliquer les présentes données SANS.

[Traduit par la Rédaction]

1. Introduction

Phospholipids are a major group of molecules found in biological membranes. They serve as selective permeability barriers between the inside and outside of cells, thus allowing for the presence of different chemical environments to optimize the cells' various functions. Because of their biocompatibility and natural tendency to form bilayered vesicles (spherical shells), phospholipids are commonly used as drug delivery carriers by encapsulating and transporting material to desired locations within cells, leading to an increase in the drug's efficacy [1–6]. However, most zwitterionic long chain lipids (i.e., > 10 hydrocarbons) self-aggregate into onion-like multilamellar vesicles (MLVs), which have a limited loading capacity, and because of their size (»100 nm), they tend to be poor drug delivery carriers owing to short circulation half-lives [7]. As a result, commonly used labour intensive processes, involving multi-stage extrusion or sonication, have been devised to produce small unilamellar vesicles (ULVs) from solutions of MLVs.

Recently, spontaneously formed ULVs have been reported in phospholipid mixtures composed of long- and short-chain lipids [8–11], and surfactants [12, 13]. These ULVs generally exhibit a narrow size distribution, endowing them with great potential in treating and diagnosing disease. In some cases, ULV radii are dependent on lipid concentration indicating that the ULV structure is not stable as a function of lipid concentration. However, there are cases where similar ULVs have been shown to be highly stable and capable of controlled-release of the encapsulated materials [14]. To better comprehend this discrepancy, a better understanding of the ULV formation mechanism is needed. In doing so, one will not only be able to streamline the production of spontaneously forming ULVs, but also provide important insights into other colloidal systems. A previous small angle neutron scattering (SANS) study indicated a strong correlation between ULV size polydispersity and ULV precursor morphologies [15]. A mechanism of ULV formation was proposed that described the transformation of discoidal bilayered micelles (commonly known as bicelles) into reasonably monodisperse ULVs. This bicelle to ULV transition, as a result of

Received 10 November 2009. Accepted 31 January 2010. Published on the NRC Research Press Web site at cjp.nrc.ca on 30 April 2010.

M.-P. Nieh[2] and N. Kučerka. Canadian Neutron Beam Centre, Steacie Institute for Molecular Sciences, National Research Council Canada, Chalk River Laboratory, Chalk River, ON K0J 1J0, Canada.
J. Katsaras. Canadian Neutron Beam Centre, Steacie Institute for Molecular Sciences, National Research Council Canada, Chalk River Laboratory, Chalk River, ON K0J 1J0, Canada; Guelph-Waterloo Physics Institute and Biophysics Interdepartmental Group, University of Guelph, Guelph, ON N1G 2W1, Canada; Department of Physics, Brock University, 500 Glenridge Avenue, St. Catharines, ON L2S 3A1, Canada.

[1]Special issue on Neutron Scattering in Canada
[2]Corresponding author (e-mail: Mu-Ping.Nieh@nrc.gc.ca).

increasing temperature, was due to bicelles coalescing and then folding onto themselves, a phenomenon driven by the loss of short-chain lipids from the bicelle's rim to either solution or the bicelle's bilayered region. Here we discuss the effects of several important parameters, such as total lipid concentration, molar ratio of long-to-short-chain lipid, lipid chain length, membrane rigidity, and charge density on ULV size to test the current model of spontaneously forming ULVs.

2. Experiment

Dihexanoyl (di-6:0; DHPC), ditridecanoyl (di-13:0; DTPC), dimyristoyl (di-14:0; DMPC), dipalmitoyl (di-16:0; DPPC) phosphatidylcholine, and dimyristoyl phosphatidylglycerol (di-14:0; DMPG) were purchased from Avanti Polar Lipids and used without further purification. Cholesterol was purchased from Sigma-Aldrich Canada Ltd., and D_2O (99.99%) from Chalk River Laboratories (Chalk River, Ont.). In one case, the lipid mixture was doped with $TmCl_3$ to study the effects of salinity and membrane charge density on the formation of ULVs. All lipids (including dopants) were first dissolved in appropriate amounts of D_2O to a total lipid concentration of 10 wt% — according to the final molar ratios (i.e., long- to short-chain lipid, charged to non-charged lipid, and dopant to lipid). Lipid mixtures were then further diluted to the desired lipid concentration with D_2O at 4 °C.

SANS measurements were carried out at the NG7 and NG3 30-m SANS instruments located at the NIST (National Institute of Standards and Technology) Center for Neutron Research (Gaithersburg, Md., USA). Sample to detector distances (SDDs) used were 1 and 4 m for the high- and mid-q [defined as $(4\pi/\lambda)\sin(\theta/2)$, where λ and θ are the wavelength and scattering angle, respectively] ranges, while the SDDs used for probing the low-q range were 15.3 and 13 m at NG7 and NG3, respectively. In all cases, 6 Å neutrons with a wavelength spread, $\Delta\lambda/\lambda$, of 15% were used. Data were collected using a 2-D detector and corrected for empty-cell scattering and background, then azimuthally averaged yielding a 1-D intensity distribution, $I(q)$. The reduced intensity data were then placed on an absolute intensity scale using the incident neutron beam flux [16].

3. SANS data analysis

Uniform-size ULVs exhibit a characteristic SANS curve (Fig. 1) containing a low-q plateau (i.e., $q < 0.006$ Å^{-1}) that is followed by oscillations, a q^{-4} decay, and a plateau region of incoherent background scattering. The low-q intensity plateau region is known as the "Guinier" regime [17], where $\log[I(q)]$ is linearly related to q^2, and the slope of the line is $-\langle L^2\rangle/3$, where $\langle L^2\rangle$ is the square average characteristic length scale of the aggregates (presumably the size of the ULVs in this case). However, depending on the length scale of interest, the Guinier regime can also be defined differently. The oscillations along the scattering curve are the result of low-polydispersity ULVs (uniform in size). At the high-q regime, the onset q value where $I(q)$ is best described by a q^{-4} decay is related to the lipid bilayer thickness (Porod's law). A detailed analysis of the bilayer form factor in this regime can be found elsewhere [18]. On the other hand,

Fig. 1. Typical SANS data of low-polydispersity ULVs (circles) at 45 °C and bicelles (triangles) at 10 °C. The data were best fit using a spherical-shell model [15] and a core-shell discoidal model [16] (solid lines).

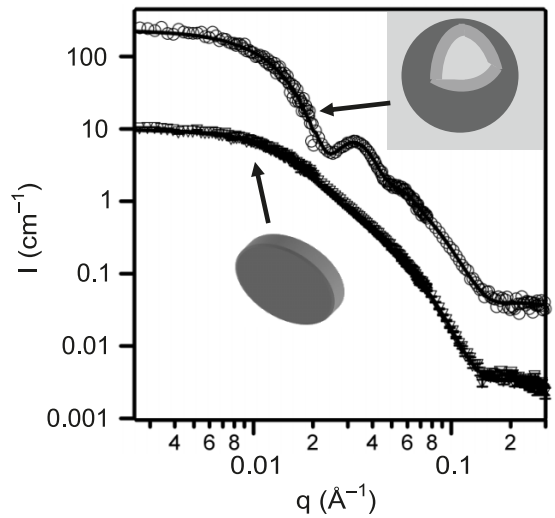

compared with ULVs, bicelles yield a distinctly different SANS pattern (Fig. 1). The bicelle SANS curve contains no oscillations, and the low-q plateau region is followed by a q^{-2} and then a q^{-4} decay, corresponding, respectively, to the bicellar planar region and the lipid bilayer itself (interface).

The structural parameters of ULVs [e.g., the average core radius $\langle R_i\rangle$, shell thickness (i.e., lipid bilayer), and ULV polydispersity] and bicelles (e.g., disk radius and bilayer thickness) can be obtained by fitting the SANS data using the appropriate model. In the case of ULVs, the most appropriate model is described by polydisperse core-shell spheres, where D_2O locates inside and outside of the hollow spheres [19, 20]. The neutron scattering length density (SLD) of the bilayer shell is simplified to be a constant, since the SLD of D2O is much higher than that of the bilayer shell. In the case of bicelles, a core-shell disk model is used to describe the core, which is composed of hydrophobic hydrocarbon chains and a shell of hydrophilic headgroups. During the fitting procedure using the NIST data analysis software (in Igor Pro) [20], both models were "smeared" by the instrumental resolution, which was calculated based on the instrument's scattering geometry and the $\Delta\lambda/\lambda$ [14]. Detailed mathematical descriptions of these models can be found elsewhere [15, 21, 22].

4. Results and discussion

Previous SANS data obtained at low temperatures (<20 °C) have indicated that the lipid mixtures in question self-aggregate into bicelles, with the long-chain lipids (e.g., DMPC, DMPG) forming the extended bilayered plane, and most of the short-chain lipid (i.e., DHPC) sequestering into the bicelle's high-curvature rim [21–23], as shown in Fig. 2. As temperature is increased, DHPC becomes not only more miscible with DMPC, but also more soluble in water, resulting in bicelles coalescing and forming larger bicelles — the result of increased line tension at the bicelle's rim. The critical size-determining stage (denoted by * in Fig. 2) occurs when bicelles stop coalescing and fold into bowl-shaped ag-

Fig. 2. Schematic describing the various morphologies as a function of temperature for a DMPC–DHPC–DMPG lipid mixture. The asterisk indicates the stage at which ULV size is determined. T^* is a function of total lipid concentration.

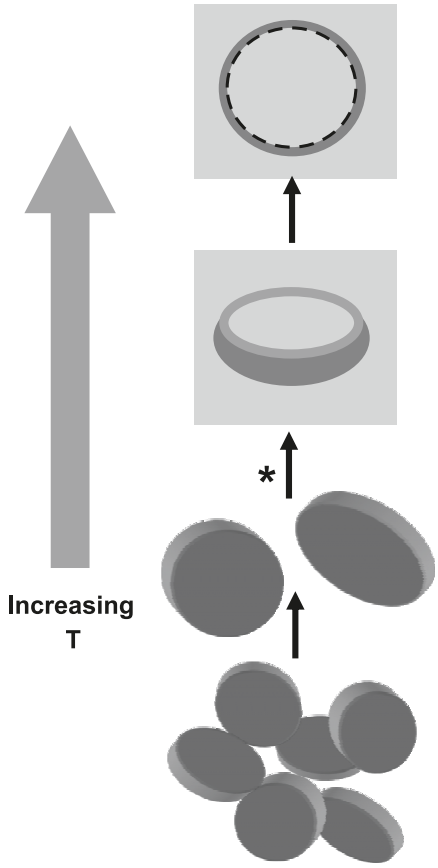

gregates at a temperature T^*. The aggregates eventually seal, forming ULVs at a temperature above the melting transition temperature, T_M, of the long-chain lipids — all lipids are now in the L_α (melted) phase and presumably completely miscible with each other. A similar mechanism of ULV formation has been proposed and experimentally studied by others [24, 25]. However, in those cases the bicelle-like aggregates were not stable, while the ones reported here (DMPC–DHPC–DMPG) are stable for a period of weeks when $T < T^*$. As a result of their stability, we are in a position to better understand the transformation of bicelles into ULVs through the detailed study of each morphology (Fig. 2). Here we investigate the effects of total lipid concentration, molar ratio of long-chain to short-chain lipid, lipid chain length, membrane rigidity, and charge density on ULV size as a function of temperature and compare with the proposed ULV mechanism of formation.

4.1 Concentration effect

An increase in total lipid concentration resulting in larger ULVs has been previously reported [10, 21]. A recent report of ULVs composed of 1.0 and 0.1 wt% DMPC–DHPC–DMPG phospholipid mixtures demonstrated ULV inner radii of 180 and 82 Å, respectively, with a bilayer thickness of 34.5 Å [14], consistent with the thickness of a DMPC bilayer at 30 °C [26]. The calculated shell volume of 1.0 wt% ULVs is about 4 times that of 0.1 wt% ULVs, implying that the average size of 1.0 wt% bicelles prior to folding (i.e., at T^*), was about 4 times that of 0.1 wt% bicelles, despite the fact that at 10 °C both samples contained bicelles of similar size. This observation is consistent with the proposed mechanism of ULV formation, in that the frequency at which bicelles coalesce (i.e., probability of collision) with each other increases with increased lipid concentration. This mechanism of formation has also been supported by recent SANS data, whereby the same lipid concentration samples produced different size ULVs depending on the annealing time of the bicelle → ULV transition [27].

Fig. 3. SANS data of a neutral Q = 3.2 and R = 0 (DMPC–DHPC) (triangles) lipid mixture, a Q = 3.2 and R = 0.067 (DMPC–DHPC–DMPG) weakly charged lipid mixture doped with $TmCl_3$ ([$TmCl_3$]/[DMPC] = 0.033) (circles), and a strongly charged Q = 3.2 and R = 0.067 (DMPC–DHPC–DMPG) lipid mixture (squares). In all cases, lipid concentration is 0.25 wt% and temperature is 45 °C. For R = 0 and 0.067 mixtures, the data were fit using the spherical-shell model. An MLV peak at $q \sim 0.1$ Å^{-1} for the neutral mixture was also observed and could not be fit by the model. The strongly charged sample showed the characteristic "bicelle" scattering pattern, the result of strong interparticle interactions. The data and fits to the data are rescaled for clarity of viewing.

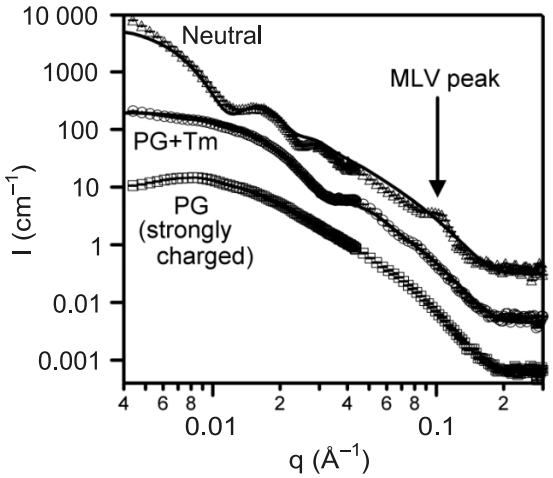

4.2 Coulombic interaction

In the case of samples with the same molar ratio of long-chain to short-chain lipid (defined as Q) = 3.2 and the same total lipid concentration (i.e., c = 0.25 wt%), but different solution charge densities and salinities, three resultant morphologies have been observed, namely MLVs, ULVs, and bicelles (Fig. 3) [11]. For zwitterionic mixtures, where R ([DMPG]/[DMPC]) is 0, and $T > T_M$ of DMPC, an oscillation along the SANS curve is observed. In addition, a peak associated with MLVs, commonly observed in pure DMPC solutions, implied the co-existence of ULVs with MLVs. However, in the case of R = 0.067 (i.e., net negative charge mixtures), bicelles persisted above T_M, presumably due to strong repulsive interactions and an increased lipid bilayer rigidity [28], preventing the bicelles from coalescing and forming ULVs. However, when the same system was doped with small amounts of $TmCl_3$ (Tm^{3+} ions strongly bind to lipid headgroups), the repulsive interaction was weakened because of Tm^{3+} ions neutralizing DMPG, resulting in low-

Fig. 4. (*a*) 10 °C and (*b*) 50 °C SANS data of DMPC–DHPC–DMPG doped with various molar ratios of cholesterol i.e., [Chol]/[DMPC]: 0 (circles), 10% (triangles), 20% (squares). At 10 °C, bicelles are present, which transform into ULVs at 50 °C. Solid curves are the best fits to the data. Best-fit parameters are tabulated in the inset to the figure.

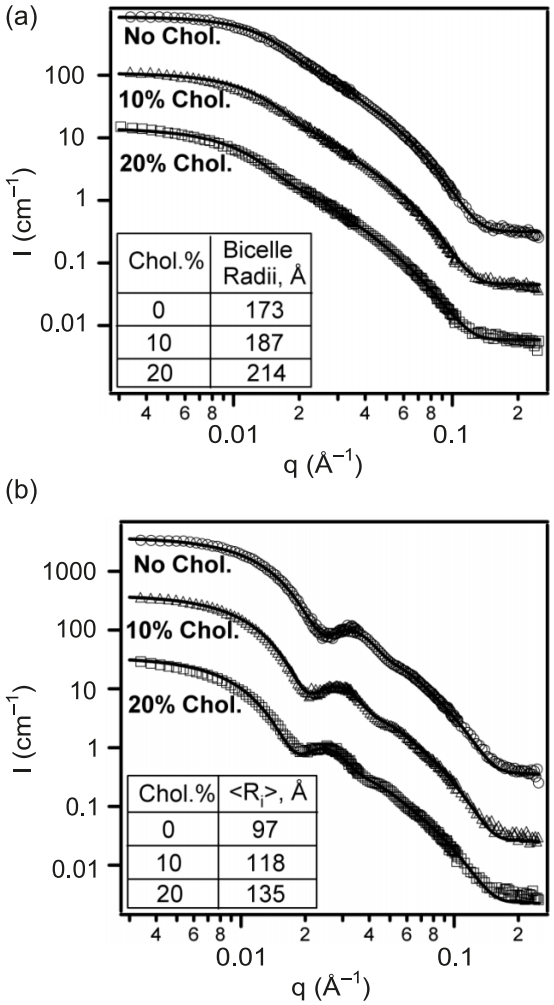

Fig. 5. SANS data of 45 °C DMPC–DHPC–DMPG ULVs at various molar ratios of long- to short-chain lipid (i.e., Q = 2.5 [triangles], 3.0 [squares], 3.5 [circles], and 4.0 [crosses]). All samples have the same total lipid concentration and R = 0.01. Best fit parameters are tabulated in the inset to the figure.

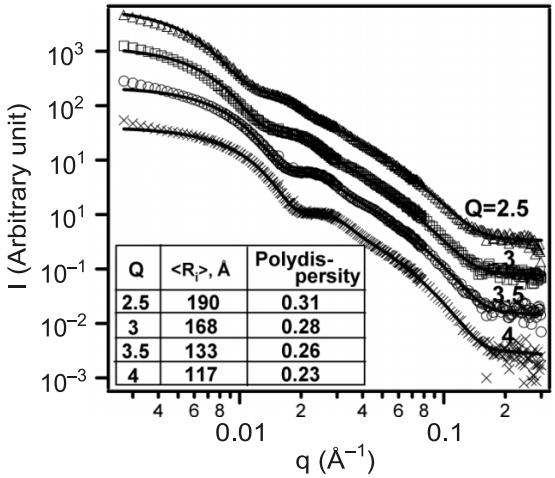

Fig. 6. SANS data of various long- and short-chain lipid mixtures with different long-chain lipids at 50 °C: DTPC (triangles), DMPC (circles), and DPPC (diamonds). Best fit core radii values and polydispersities are tabulated in the inset to the figure.

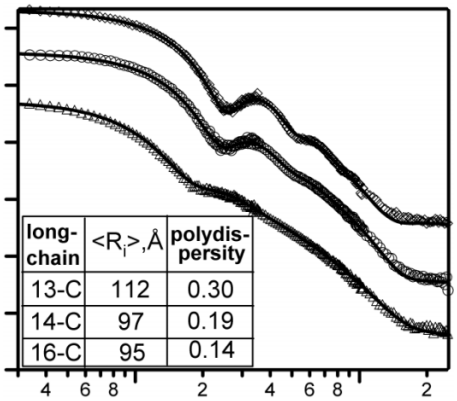

polydispersity ULVs above T_M. Again, this result is in support of the proposed mechanism of ULV formation.

In comparison, a previous study on the same lipid mixture produced an unexpected result, namely that salinity did not play an important role in ULV size [29]. However, this result could possibly be attributed to the narrow range of salinities studied.

4.3 Membrane rigidity

It is well-known that cholesterol increases rigidity of fluid membranes through increased molecular ordering [30, 31]. SANS data of a common ULV system (total lipid concentration = 0.1 wt%), composed of DMPC, DMPG, and DHPC (Q = 3.2, R = 0.01), and doped with various amounts of cholesterol (i.e., [Chol]/[DMPC] = 0, 10%, 20%) are shown in Fig. 4. The morphologies exhibited by the three mixtures, i.e., bicelles at 10 °C [Fig. 4*a*] and ULVs at 50 °C [Fig. 4*b*], are consistent with previous reports [21–23]. Best fits of bicelle data (i.e., at 10 °C) resulted in radii of 173, 187, and 214 Å, for [Chol]/[DMPC] = 0, 10%, and 20%, respectively, and a bilayer thickness ~44 Å. Best fits of corresponding 50 °C data resulted in ULV core radii, $\langle R_i \rangle$, of 97, 118, and 135 Å, with a bilayer thickness of 34 Å. The best fit bilayer thickness data, however, are not sensitive to cholesterol content as previously reported [32], possibly due to the rudimentary model used to fit the data. The size of ULVs is dictated by the initial bicelle size, which increases with higher cholesterol content as a result of increased hydrophobic content, consistent with the proposed mechanism of ULV formation. Although the number of short-chain DHPC molecules for any given morphology is considered to be variable due to differing solubilities as a function of temperature, the number of long-chain lipids (i.e., DMPC) was assumed to be constant, and as such proportional to the bilayer's surface area (i.e., the total bilayer headgroup area). In the case of bicelles, the calculated bilayer surface areas for 0, 10%, and 20% [Chol]/[DMPC] are 1.9×10^5, 2.2×10^5, and 2.9×10^5 Å^2, respectively, while for the same [Chol]/[DMPC] ratios, ULV surface areas are 3.3×10^5, 4.7×10^5, and 5.8×10^5 Å^2, respectively. The fact that the

number of bicelles coalescing into precursors increases weakly with increased cholesterol content is indicative of the reluctance of bicelles to fold at higher cholesterol content.

4.4 Q value

A previous study on the effect of long-chain to short-chain lipid molar ratios (i.e., Q) on ULV size (Fig. 5) indicated that a higher Q systematically resulted in smaller radius ULVs [33]. This was explained by the paucity of DHPC to stabilize the bicelle morphology in the cases of higher Q samples (for the same size of bicelles), thus accelerating the folding process and promoting the formation of smaller ULVs. The fact that the polydispersity of the higher-Q ULVs is smaller, also suggests a shorter coalescence time leading to more uniform size ULVs.

4.5 Length of the long-chain lipid

To understand the effect of hydrocarbon chain length on ULV size, various long-chain lipids were employed for lipid mixtures with Q of 3.2, a total lipid concentration of 0.1 wt%, and a constant charge density of R = 0.01. It should be pointed out that the long-chain and short-chain lipids must be in the gel and L_α phases, respectively, in order for bicelles to form. As a result, the shortest long-chain lipid chosen was DTPC (di-13:0, with $T_M \sim 14$ °C). SANS data, shown in Fig. 6, indicate that all lipid mixtures [i.e., DTPC (di-13:0), DMPC (di-14:0), and DPPC (di-16:0)] form ULVs with $<R_i>$ of 112, 97, and 95 Å for DTPC, DMPC, and DPPC mixtures, respectively. This weak dependence of ULV size on hydrocarbon chain length is presumably the result of a number of counter-balancing factors. As expected, compared with the longer-chain DPPC lipid, the shorter-chain DTPC lipid forms a thinner bilayer (i.e., bilayer thickness ~26 vs. 39 Å). The best fit thickness for the DTPC bilayer is slightly smaller than the expected value of ~33 Å [26], while that for DPPC is consistent with the literature value of 39 Å [34]. The difference in bilayer thickness implies that only 2/3 of the DHPC is needed to stabilize the same radius bicelles, with the result of bicelles that fold at a slower rate. On the other hand, DTPC bilayers are less rigid (with shorter hydrocarbon chains) and are thus easier to fold into ULVs. However, based on the $<R_i>$ data, it seems that the latter plays a lesser role in ULV formation. Finally, compared with DPPC ULVs, ULVs containing DTPC are less uniform in size (30% for DTPC vs. 14% for DPPC ULVs). This may be explained if DTPC bicelles fold into ULVs at a slower rate, thus leading to a greater variation in size.

5. Conclusion

SANS data show how various physical parameters can affect the size of spontaneously forming ULVs. The current data are best explained by a previously proposed mechanism for ULV formation [15, 24], in which the precursor morphology is uniform-size self-assembled bicelles whose origin of formation is yet to be understood. This elevated understanding of ULV formation can lead to practical applications, especially with regards to the production of ULVs as diagnostic and therapeutic carriers.

Acknowledgement

This work utilized facilities supported in part by the National Science Foundation under Agreement No. DMR-9986442.

References

1. D.C. Drummond, O. Meyer, K. Hong, D.B. Kirpotin, and D. Papahadjopoulos. Pharmacol. Rev. **51**, 691 (1999). PMID: 10581328.
2. M. Voinea and M. Simionescu. J. Cell. Mol. Med. **6**, 465 (2002). doi:10.1111/j.1582-4934.2002.tb00450.x. PMID: 12611636.
3. M. Hashida, S. Kawakami, and F. Yamashita. Chem. Pharm. Bull. (Tokyo), **53**, 871 (2005). doi:10.1248/cpb.53.871. PMID:16079512.
4. G. Sharma, S. Anabousi, C. Ehrhardt, and M.N. Ravi Kumar. J. Drug Target. **14**, 301 (2006). doi:10.1080/10611860600809112. PMID:16882550.
5. M.T. Krauze, J. Forsayeth, J.W. Park, and K.S. Bankiewicz. Pharm. Res. **23**, 2493 (2006). doi:10.1007/s11095-006-9103-5. PMID:16972184.
6. T. Ishida, Y. Takanashi, and H. Kiwada. Biol. Pharm. Bull. **29**, 397 (2006). doi:10.1248/bpb.29.397. PMID:16508135.
7. R.L. Juliano and D. Stamp. Biochem. Biophys. Res. Commun. **63**, 651 (1975). doi:10.1016/S0006-291X(75)80433-5. PMID:1131256.
8. P. Schurtenberger, N. Mazer, and W. Kaenzig. J. Phys. Chem. **89**, 1042 (1985). doi:10.1021/j100252a031.
9. R.P. Hjelm, M.H. Alkan, and P. Thiyagarajan. Mol. Cryst. Liq. Cryst. (Phila. Pa.), **180**, 155 (1990). doi:10.1080/00268949008025796.
10. J. Oberdisse and G. Porte. Phys. Rev. B, **56**, 1965 (1997).
11. M.-P. Nieh, T.A. Harroun, V.A. Raghunathan, C.J. Glinka, and J. Katsaras. Biophys. J. **86**, 2615 (2004). doi:10.1016/S0006-3495(04)74316-7.
12. M.A. Kiselev, D. Lombardo, P. Lesieur, A.M. Kisselev, S. Borbely, T.N. Simonova, and L.I. Barsukov. Chem. Phys. **345**, 173 (2008). doi:10.1016/j.chemphys.2007.09.034.
13. P. Lesieur, M.A. Kiselev, L.I. Barsukov, and D. Lombardo. J. Appl. Cryst. **33**, 623 (2000). doi:10.1107/S0021889899012765.
14. M.-P. Nieh, J. Katsaras, and X. Qi. Biochim. Biophys. Acta, Biomembr. **1778**, 1467 (2008). doi:10.1016/j.bbamem.2008.02.016.
15. M.-P. Nieh, V.A. Raghunathan, S.R. Kline, T.A. Harroun, C.Y. Huang, J. Pencer, and J. Katsaras. Langmuir, **21**, 6656 (2005). doi:10.1021/la0508994. PMID:16008370.
16. C.J. Glinka, J.G. Barker, B. Hammouda, S. Krueger, J.J. Moyer, and W.J. Orts. J. Appl. Cryst. **31**, 430 (1998). doi:10.1107/S0021889897017020.
17. J.S. Higgins and H.C. Benoit. Polymers and Neutron Scattering. Chap. 6. Clarendon Press, Oxford. 1994.
18. N. Kučerka, J.F. Nagle, S.E. Feller, and P. Balgavý. Phys. Rev. E Stat. Nonlin. Soft Matter Phys. **69**, 051903 (2004). PMID:15244843.
19. J.B. Hayter. *In* Physics of amphiphiles-micelles, vesicles, and microemulsions. *Edited by* V. Degiorgio and M. Corti. Determination of structure and dynamics of micellar solutions by neutron small angle scattering, Amsterdam. 1985. pp. 60–93.
20. S.R. Kline. J. Appl. Cryst. **39**, 895 (2006). doi:10.1107/S0021889806035059.
21. M.-P. Nieh, C.J. Glinka, S. Krueger, R.S. Prosser, and J.

Katsaras. Langmuir, **17**, 2629 (2001). doi:10.1021/la001567w.
22. M.-P. Nieh, C.J. Glinka, S. Krueger, R.S. Prosser, and J. Katsaras. Biophys. J. **82**, 2487 (2002). doi:10.1016/S0006-3495(02)75591-4. PMID:11964236.
23. J. Katsaras, T.A. Harroun, J. Pencer, and M.-P. Nieh. Naturwissenschaften, **92**, 355 (2005). doi:10.1007/s00114-005-0641-1. PMID:16021408.
24. J. Leng, S.U. Egelhaaf, and M.E. Cates. Biophys. J. **85**, 1624 (2003). doi:10.1016/S0006-3495(03)74593-7. PMID:12944278.
25. St. Schmölzer, D. Gräbner, M. Gradzielski, and T. Narayanan. Phys. Rev. Lett. **88**, 258301 (2002). doi:10.1103/PhysRevLett.88.258301. PMID:12097133.
26. N. Kučerka, Y. Liu, N. Chu, H.I. Petrache, S. Tristram-Nagle, and J.F. Nagle. Biophys. J. **88**, 2626 (2005). doi:10.1529/biophysj.104.056606. PMID:15665131.
27. S. Mahabir, W. Wan, J. Katsaras, and M.-P. Nieh. J. Phys. Chem. B. In press.
28. L.M. Bergström. Langmuir, **22**, 6796 (2006). doi:10.1021/la060520t. PMID:16863224.
29. B. Yue, C.-Y. Huang, M.-P. Nieh, C.J. Glinka, and J. Katsaras. J. Phys. Chem. B, **109**, 609 (2005). doi:10.1021/jp047510q. PMID:16851053.
30. J.M. Boggs and J.C. Hsia. Biochim. Biophys. Acta, Biomembr. **290**, 32 (1972). doi:10.1016/0005-2736(72)90049-1.
31. R. Mendelsohn. Biochim. Biophys. Acta, Biomembr. **290**, 15 (1972). doi:10.1016/0005-2736(72)90047-8.
32. J. Pencer, M.-P. Nieh, T.A. Harroun, S. Krueger, C. Adams, and J. Katsaras. Biochim. Biophys. Acta, Biomembr. **1720**, 84 (2005). doi:10.1016/j.bbamem.2005.10.017.
33. M.-P. Nieh, V.A. Raghunathan, C.-Y. Huang, J. Pencer, T.A. Harroun, and J. Katsaras. NSTI Nanotech Technical Proceedings, **2**, 709 (2006).
34. N. Kučerka, J.F. Nagle, J.N. Sachs, S.E. Feller, J. Pencer, A. Jackson, and J. Katsaras. Biophys. J. **95**, 2356 (2008). doi:10.1529/biophysj.108.132662. PMID:18502796.